Japan-US Interdisciplinary Program Emphasizing Student Academic Growth
AY 2026 Global Steam Exchange Project for NU Engineering Students

Individual Activity Report

Yupeng Li
New York University Mechanical Engineering, Junior
yl11710@nyu.edu

BACKGROUND AND STUDY GOALS FOR THE PROGRAM

Mechanical engineering increasingly requires the integration of structural design, electronics, sensing, actuation, and control. Previous academic and project experience in computer-aided design (CAD), rapid prototyping, and robotics provided a foundation for participation in the SILP glider project. Particular interest was placed on aerodynamic design and the interaction between the physical airframe and its control system.

The SILP program offered an opportunity to study these areas through the design, fabrication, and testing of a small glider. The completed glider was intended for flight in a student competition held at Gifu University. Therefore, the project required consideration of aerodynamics, structural weight, manufacturing limitations, sensor measurements, actuator behavior, reliability, and flight stability.

A primary objective of the program was to investigate the aerodynamic and mechanical design of the glider. Factors such as wing geometry, center-of-gravity location, structural stiffness, tail configuration, and weight distribution were considered because of their influence on stability and glide performance.

Another study goal was to examine how mechanical design affects the control system. Wing alignment, balance, tail geometry, and servo neutral position can significantly influence flight behavior, while software alone cannot fully correct an improperly designed or misaligned airframe.

Control-engineering principles were then applied to improve flight stability. Accelerometer and gyroscope measurements were used to estimate roll and pitch, and the resulting attitude errors were used to command the elevator and rudder servos through proportional feedback control. The program also provided experience in technical collaboration within an international laboratory environment.

ACTIVITIES OUTLINE

Preliminary Design and Project Requirements

The project began with a review of the glider requirements and the available manufacturing resources [4]. The completed glider was required to fit inside a provided suitcase measuring 70 cm × 45 cm × 30 cm. The main design priorities were stable gliding performance, low structural weight, ease of manufacturing, and compatibility with an active flight-control system.

Based on these requirements, an aspect ratio of 6.25 was selected as a practical balance between aerodynamic efficiency, structural integrity, and ease of construction. The primary design parameters were discussed with the teaching assistants and finalized as summarized in Table 1.

Table 1: Preliminary Glider Design Parameters

Wingspan (b)	1.00 m
Chord Length (c)	0.160 m
Aspect Ratio (AR)	6.25
Main Wing Area (S)	0.16 m^2
Dihedral Angle	7°
Target Mass (m)	220 g
Horizontal Tail Volume Target (V_h)	0.40
Vertical Tail Volume Target (V_f)	0.02
Tail Moment Arm (l_h & l_f)	0.50 m

The required horizontal- and vertical-tail areas were estimated using the selected tail-volume coefficients. The horizontal-tail area was calculated as

$$S_h = \frac{V_h * S * c}{l_h} = \frac{0.4 * 0.16m^2 * 0.16m}{0.5m} = 0.0205m^2 \quad (1)$$

The vertical-tail area was calculated as

$$S_f = \frac{V_f * S * b}{l_f} = \frac{0.02 * 0.16m^2 * 1m}{0.5m} = 0.0064m^2 \quad (2)$$

These calculations provided preliminary target areas for the horizontal and vertical stabilizers. The final tail geometry was then developed to approximately satisfy these areas while remaining compatible with the airframe structure, control surfaces, and suitcase-size constraint.

Aerodynamic Configuration

The purpose of the airfoil-selection process was to obtain a high lift-to-drag ratio under the expected low-speed operating conditions. A flight velocity of 6 m/s was assumed for the preliminary aerodynamic calculations. The required lift coefficient was calculated from

$$C_L = \frac{2W}{\rho V^2 S} = \frac{2*0.22kg*9.81\frac{m}{s^2}}{1.2\frac{kg}{m^3}*(6\frac{m}{s})^2*(0.16m^2)} = 0.62 \quad (3)$$

The Reynolds number based on the wing chord was calculated as

$$Re = \frac{\rho V c}{\mu} = \frac{1.2\frac{kg}{m^3}*6\frac{m}{s}*0.16m}{1.8*10^{-5}\,Pa*s} = 64000 \quad (4)$$

These calculations were based on the preliminary target mass of 220 g. At the assumed flight speed of 6 m/s, the preliminary design required a lift coefficient of approximately 0.62. The completed competition glider had a higher mass of approximately 340 g and would therefore require a lift coefficient of approximately 0.97 at the same speed. The preliminary calculation was retained as the basis for the initial aerodynamic design and airfoil selection. The Reynolds number remained approximately 64,000 because it depended on the flight speed, chord length, and air properties rather than the glider mass. Based on the available airfoil-polar data, the AG03 airfoil was selected because it demonstrated favorable aerodynamic performance at low Reynolds numbers. Its geometry was compared with the commonly used Clark Y airfoil, as shown in Figure 1 [1].

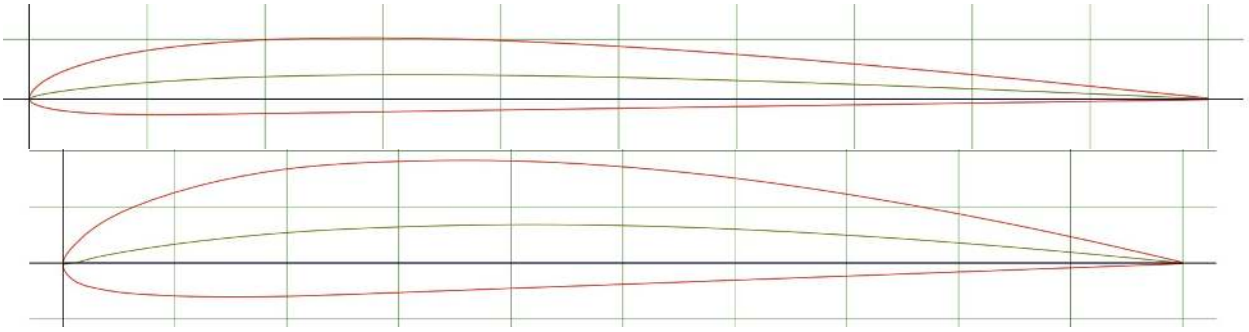


Figure 1: AG03 Airfoil Profile (Top) and Clark Y Airfoil Profile (Bottom) [1]

The aerodynamic performance of the two airfoils was then compared using their lift-to-drag ratio, CL/CD, over a range of angles of attack. At Re=50,000, represented by the blue curves in Figure 2, the AG03 exhibited a higher lift-to-drag ratio than the Clark Y airfoil under the expected low-speed operating conditions。

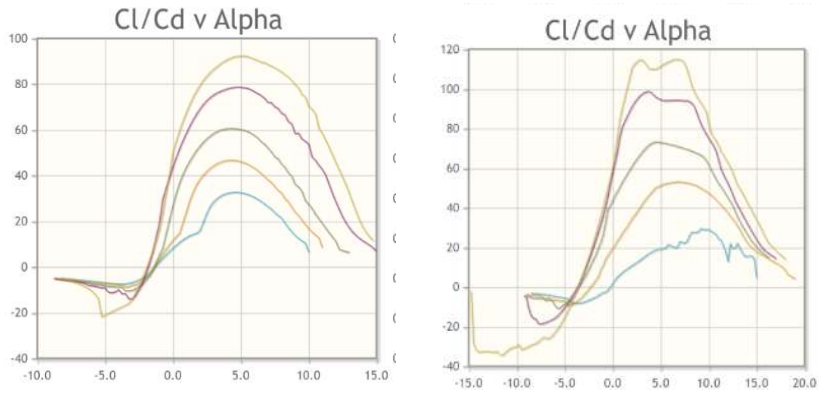


Figure 2: Cl/CD Versus Angle of Attack (Alpha) Plot of AG03 Airfoil (Left) and Clark Y (Right) [1]

The C_L versus angle of attack curve also indicated that a C_L of approximately 0.6 to 0.7 could be achieved at an angle of attack of around 3° to 5° (Figure 3).

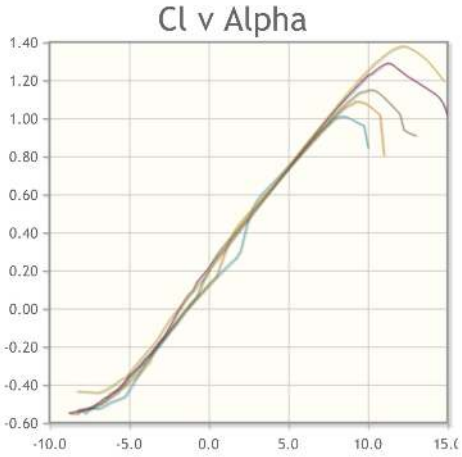


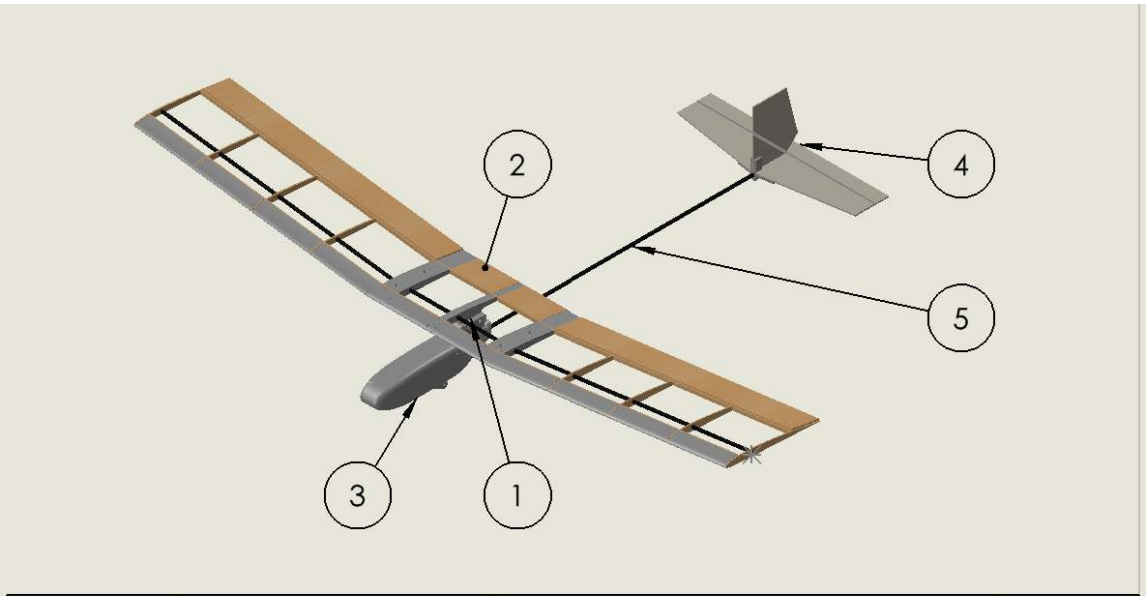
Figure 3: Cl Versus Angle of Attack (Alpha) Plot of AG03 [1]

Therefore, the AG03 was considered suitable for the expected low-speed flight condition.

Mechanical Design and Manufacturing

The aerodynamic configuration established in the preliminary design stage was then converted into a manufacturable airframe using SOLIDWORKS Education Edition [2]. To satisfy the transportation constraint imposed by the suitcase while maintaining a 1.0 m wingspan, the glider was designed as a detachable structure. The main airframe consisted of a main wing, nose

section, tail boom, and tail-wing assembly. Lightweight construction and structural rigidity were prioritized to support stable low-speed flight (Figure 4).



ITEM NO.	PART NUMBER	DESCRIPTION	QTY.
1	Angler4	PLA: Adjusts Wing Angle of Attack	1
2	Mainwing	PLA, Carbon Fiber, Balse/Birch Wood	1
3	Nose	PLA: Contains Eletronics	1
4	Tail_Wings	Styrofoam: Controls Flight	1
5	TailRod	Carbon Fiber: Provides Rigidity	1

Figure 4: Isometric Assembly With Labeled Parts and Materials

The nose section housed the electronic components, while the carbon-fiber tail boom connected the main airframe to the tail assembly and provided bending rigidity with limited additional mass. Lightweight foam was used for the horizontal and vertical tail surfaces to reduce aft weight and improve center-of-gravity adjustment.

The main wing was designed with a total span of 1.0 m and a constant chord of 0.160m. To allow disassembly for transport, the wing was divided into three sections, consisting of a 0.2m center section and two 0.4m outer sections. A dihedral angle of 7° was introduced in the two outer wing panels to improve passive roll stability. The tail assembly was positioned at a moment arm of approximately 0.5m from the main wing in accordance with the preliminary tail-sizing calculations (Figure 5).

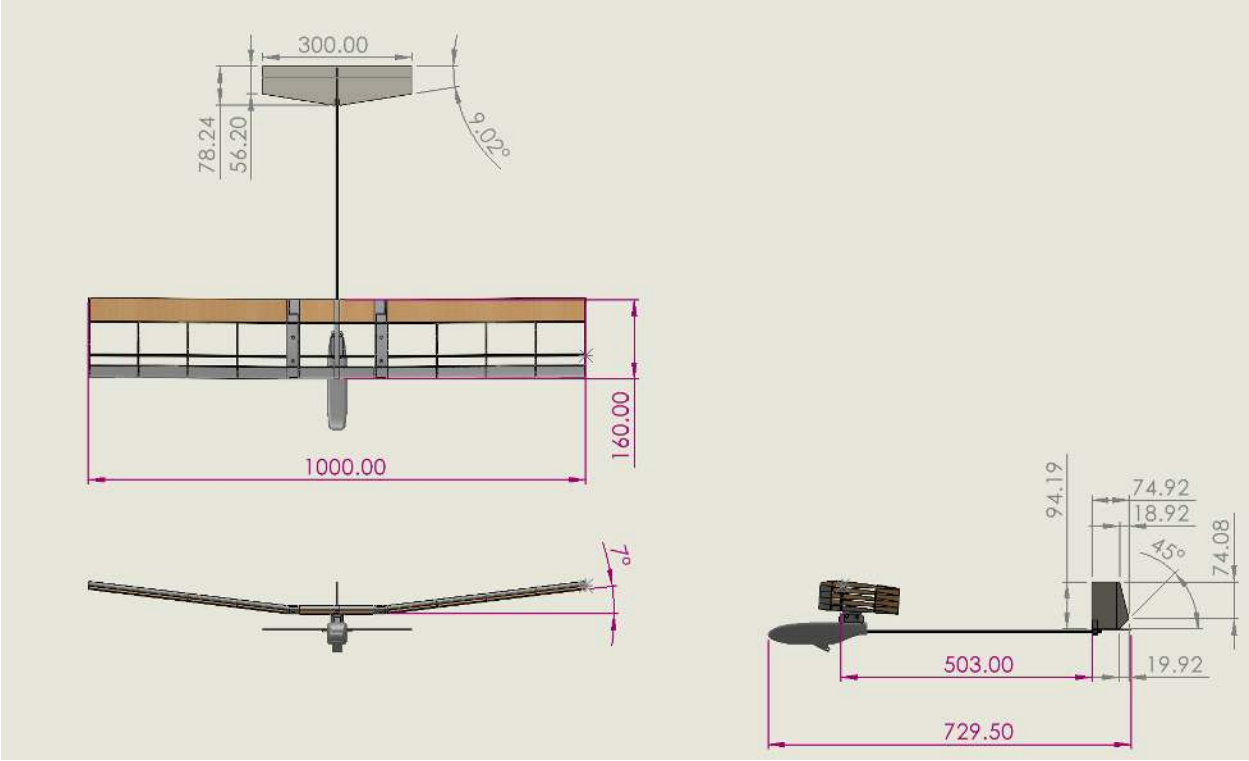
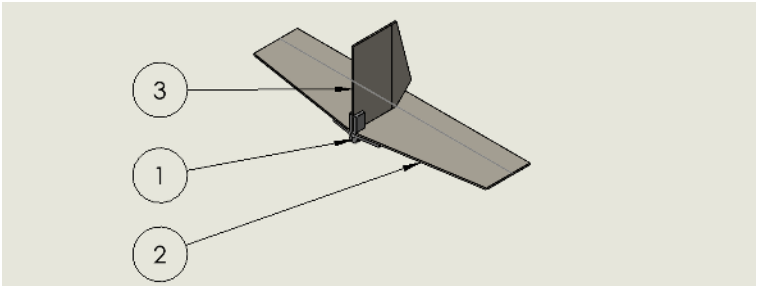


Figure 5: Three-view Drawing of Glider

The tail surfaces were designed to approximately satisfy the calculated horizontal- and vertical-tail target areas of 0.0205 m^2 and 0.0064 m^2 respectively. The horizontal tail incorporated an elevator for pitch control, while the vertical tail incorporated a rudder for directional control. Both surfaces were manufactured from lightweight styrofoam to reduce aft mass. A PLA tail attachment was used to align the two surfaces and connect the tail assembly to the carbon-fiber tail boom (Figure 6).



ITEM NO.	PART NUMBER	DESCRIPTION	QTY.
1	Tail Attachment	PLA Connects w/Nose	1
2	Horizontal Tailwing	Styrofoam: Elevator	1
3	Vertical Tail Wing	Styrofoam: Rudder	1

Figure 6: Tail Assembly

The center-wing connection was designed to maintain alignment between the horizontal center panel and the two dihedral outer panels. The detachable parts were secured using two M3 countersunk bolts with lengths of 10 mm and 8 mm. Hexagonal nut pockets were incorporated on the opposite side of the connection to retain the nuts and prevent rotation during tightening. The countersunk bolt heads remained approximately flush with the surrounding surface, while the nut pockets provided a secure and repeatable connection. This fastening arrangement allowed the wing sections to be assembled rigidly for flight and removed for transportation (Figure 7).

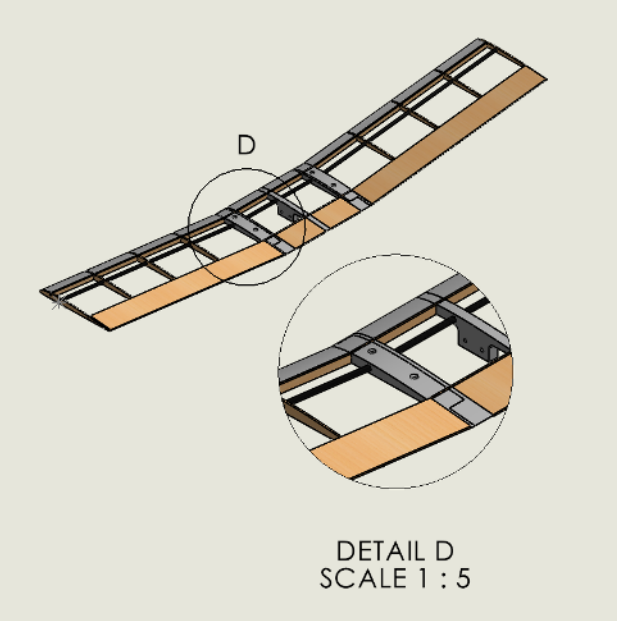


Figure 7: Detailed View of the Center Wing Connections

The main wing used laser-cut birch ribs spaced 10 cm apart, supported by a carbon-fiber spar and longitudinal wooden members. More complex parts, including the wing-angle connector and nose housing, were produced using PLA 3D printing.

Before final assembly, the wing joints, spar openings, bolt holes, and nut pockets were test-fitted and adjusted where necessary. This ensured accurate alignment and secure assembly of the detachable components.

After the internal wing structure was assembled, the main wing was covered with heat-shrink film to create a smooth aerodynamic surface while adding minimal mass. The film was carefully tensioned and heated around the ribs and supporting members to reduce wrinkles and preserve the AG03 airfoil profile (Figure 8).

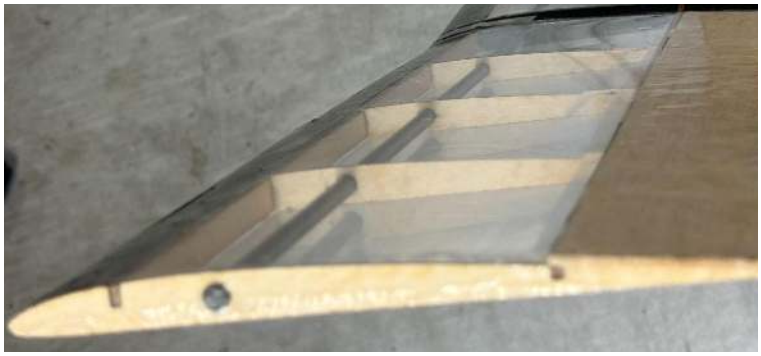


Figure 8. Main Wing with Heat Shrink Film

Following completion of the wing covering, the main wing, fuselage, nose section, tail boom, and tail surfaces were assembled into the final glider configuration (Figure 9).

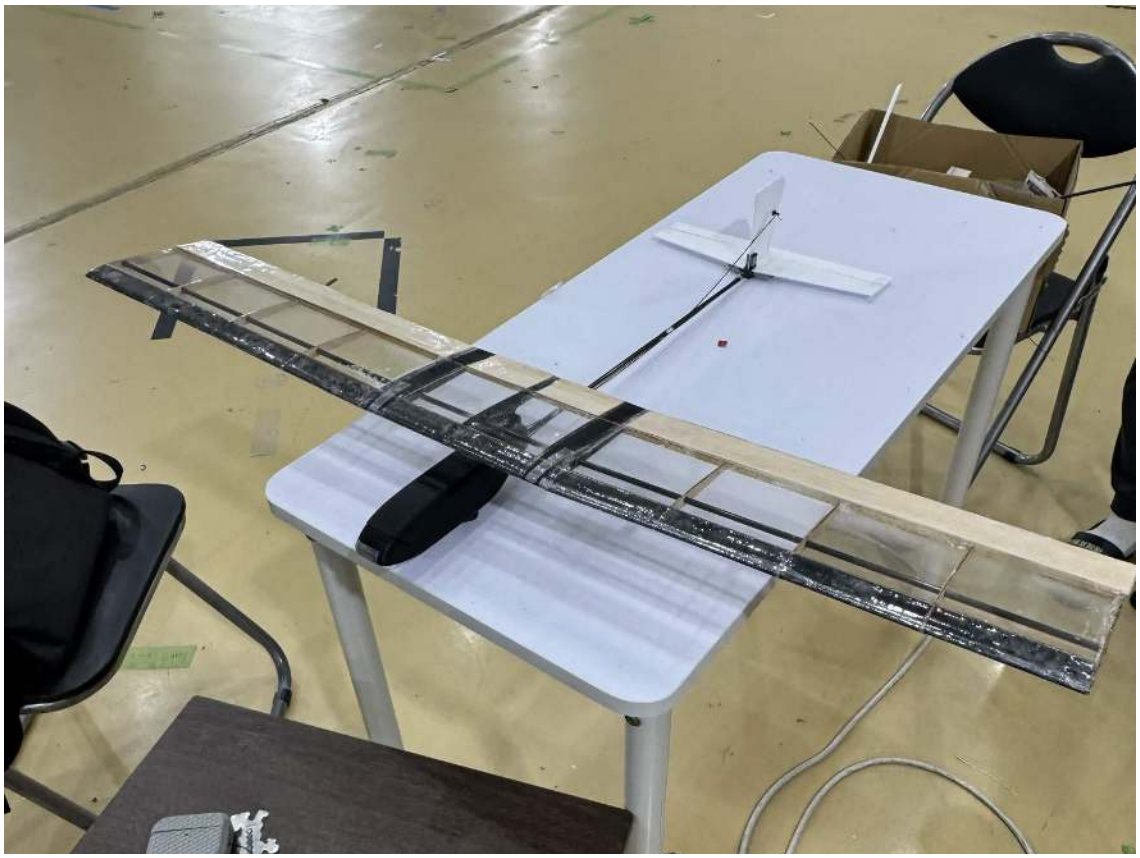


Figure 9: Fully assembled Glider

The completed airframe combined laser-cut wooden components, styrofoam tail surfaces, PLA 3D-printed parts, carbon-fiber reinforcement, mechanical fasteners, and heat-shrink-film covering. The final structure remained detachable for transportation while maintaining sufficient rigidity for flight testing.

Sensor, Servo, and Control-System Integration

The active flight-control system consisted of a microcontroller with an integrated inertial measurement unit, two servo motors, a battery supply, and the required wiring and mechanical linkages. Utilizing the Arduino IDE, the microcontroller processed the measured glider attitude and generated commands for the elevator and rudder servos [3].

Table 2: Main Electronic and Control Components

Components	Quantity	Function
Seeed Studio XIAO nRF52840 Sense with built-in LSM6DS3TR-C IMU	1	Reads acceleration and angular velocity, estimates attitude, and generates servo commands
Elevator Servo 3.5g	1	Adjusts the horizontal-tail control surface
Rudder Servo 3.5g	1	Adjusts the vertical-tail control surface
3.7 V Li-Po Battery and Power Wiring	1 Set	Supplies power to the controller and servos
Steel pushrods and Hooks	2 Sets	Transfer servo motion to the elevator and rudder

Two servo motors were installed near the tail-control mechanism. Steel pushrods connected the servo arms to control hooks attached to the elevator and rudder. Rotation of each servo arm produced linear pushrod motion, which rotated the corresponding control surface about its hinge. The linkage positions were adjusted manually to establish the neutral elevator and rudder positions before electronic calibration (Figure 10).

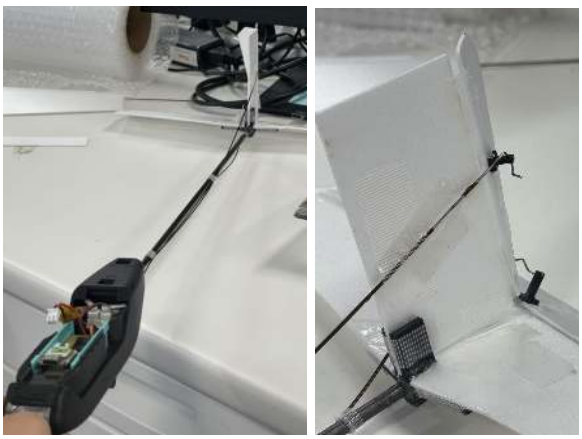


Figure 10: Mechanical Servo Linkage and Control Hooks

The linkage geometry allowed the rudder to move approximately 40° to the left and right and the elevator to move approximately 40° upward and downward. Mechanical movement was

checked before powered testing to ensure that the surfaces did not contact the tail structure or place excessive load on the servos.

Each servo was calibrated by identifying its neutral position and safe operating limits. The elevator servo was connected to pin D1, while the rudder servo was connected to pin D2. The command limits of the servo motor were manually calibrated and noted in Table 3.

Table 3: Servo Command Parameters

Control Surface	Pin	Neutral Command	Command Limits
Elevator	D1	100°	60° to 135°
Rudder	D2	97°	60° to 140°

These software limits prevented the servos from forcing the control surfaces beyond their mechanically allowable ranges.

The XIAO nRF52840 Sense includes a built-in LSM6DS3TR-C six-axis IMU containing a three-axis accelerometer and three-axis gyroscope. The measurements were processed using the Madgwick filter to estimate the glider's roll and pitch angles. Before launch, the system was reset while the glider was held at the desired initial attitude, establishing the reference condition for the controller, as shown in Figure 11.

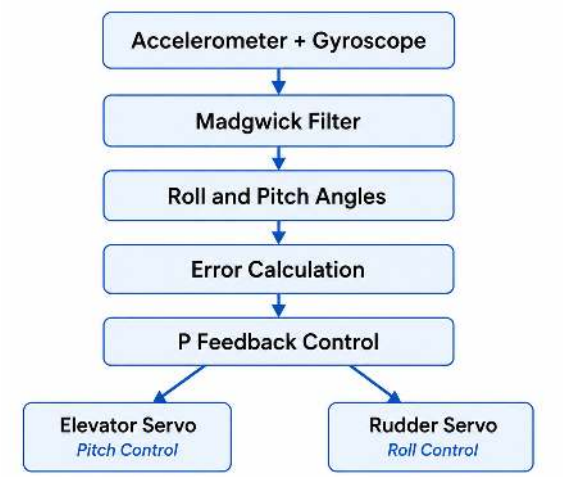


Figure 11: Block Diagram of the IMU-Based Proportional Flight-Control System

The roll and pitch angles estimated by the Madgwick filter were compared with reference angles recorded before launch. The glider was held at the desired initial attitude and reset, establishing the reference roll angle, ϕ_0, and pitch angle, θ_0. The attitude errors were then calculated as

$$e_{\phi} = \phi - \phi_0 \quad (5)$$

$$e_{\theta} = \theta - \theta_0 \quad (6)$$

where e_{ϕ} and e_{θ} represent the roll and pitch errors, respectively.

Proportional feedback control was used to generate the servo commands:

$$u_e = u_{e0} + K_{p\theta} e_{\theta} \quad (7)$$

$$u_r = u_{r0} + K_{p\phi} e_{\phi} \quad (8)$$

where u_e and u_r are the elevator and rudder servo commands, u_{e0} and u_{r0} are the calibrated neutral commands, and $K_{P\theta}$ and $K_{P\phi}$ are the proportional gains. Pitch error controlled the elevator, while roll error controlled the rudder. The gain directions were selected so that the control surfaces opposed the measured attitude error.

The calculated commands were restricted to the servo limits listed in Table 3. This prevented the elevator and rudder from exceeding their mechanically allowable ranges. Direct yaw feedback was not used because the six-axis IMU did not provide an absolute yaw reference.

Testing and Iterative Modification

Flight testing was conducted indoors under approximately still-air conditions. The glider was launched from a flat wooden guide using a horizontally stretched rubber band connected to a pull rope. The glider was positioned on the guide, the rubber band was pulled backward, and the system was released to provide a repeatable forward launch. Initial tests used lower launch tension, which was gradually increased after confirming that the structure and control surfaces operated safely (Figure 12).

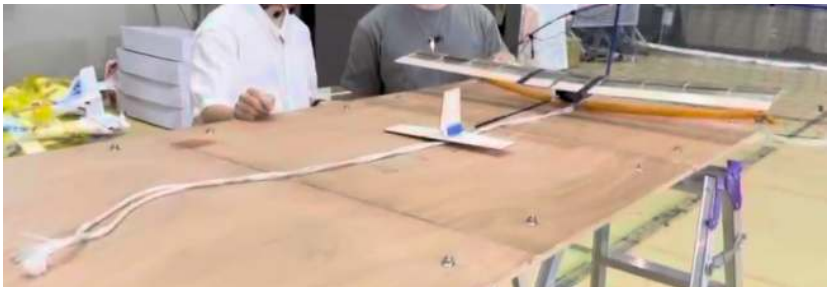


Figure 12: Indoor Rubber-Band Launch Setup Used for Flight Testing

The first glider configuration had a mass of approximately 380 g, used balsa-wood tail surfaces, and did not include active feedback control. Its center of mass was located approximately 8 cm aft of the intended 30%-chord position. After launch, the glider pitched upward rapidly, lost airspeed, and stalled. The nose then rotated downward, resulting in a steep descent. This behavior indicated insufficient longitudinal stability caused primarily by the excessively aft center-of-mass position.

Following the initial test, the glider mass was reduced to approximately 340 g by replacing the balsa-wood tail surfaces with styrofoam components and reducing the printing density of the PLA parts. The center of mass was also moved forward to the intended 30%-chord location, and the active feedback-control system was enabled. The proportional gains were adjusted through repeated testing, with final values of

$$K_{P\theta} = 5 \tag{9}$$

for elevator-based pitch control and

$$K_{P\phi} = 2 \tag{10}$$

for rudder-based roll correction.

During the second major test, the glider traveled across the testing area and reached the opposite side of the room. The flight ended when the tail contacted an obstacle and the 2mm styrofoam tail surface fractured. Although the lighter tail reduced the total mass, the damage showed that the selected foam thickness provided limited impact resistance. Wing-incidence adjustment components ranging from 2° to 6° were fabricated and evaluated during indoor testing. The 3° incidence setting produced the most stable glide and was selected for the competition configuration. Because several modifications were introduced simultaneously, the improvement could not be attributed to the feedback controller alone.

FINDINGS AND RESULTS

On July 10, the completed glider was evaluated at a flight competition held at Gifu University alongside five other university teams. Each team was allowed five launch attempts, with the option to conduct the flight with or without an applied disturbance. The launch setting was adjusted between attempts to identify a suitable initial speed.



Figure 13: Gifu University Glider Launch Setup

The competition launcher used a thinner release string than the rope used during the earlier indoor tests. Although the thinner string reduced resistance during release, it could more easily enter gaps around the tail surfaces and control linkages. This created a greater risk of the string becoming caught during launch.

Table 4. Summary of Competition Flight Attempts

Attempt	Launch Setting	Result
1	~70	Insufficient launch force; glider did not leave the launcher successfully
2	~170	Successful glide; the spare wing was installed before the next attempt.
3	~200	Best flight of approximately 35 m; glider turned near the end
4	Not Recorded	Launch string caught the tail assembly and caused structural damage
5	Not Recorded	After repair, string interference occurred again; final flight was conducted without active control after the linkage hook was lost

The third attempt produced the best result, with the glider traveling approximately 35 m. The flight remained stable with slight oscillation through most of its trajectory but turned toward the corner of the testing area as it slowed near the end. Possible causes included reduced rudder effectiveness at low speed, a small rudder-neutral offset, or minor wing and tail misalignment.

The later attempts revealed a limitation in the mechanical integration between the glider and the launching system. The thin release string became caught around the tail region, damaging the tail structure and control linkage. Although repairs were attempted, the loss of the mechanical linkage hook prevented normal operation of the active control system. These results showed that future designs should provide greater clearance around the tail, shield the control linkages, or reposition the release string to reduce the risk of interference.

FURTHER APPLICATION OF PROGRAM OUTCOME

The program provided practical experience in integrating aerodynamic design, lightweight structures, sensing, actuation, and feedback control within one engineering system. These skills can be applied to future work in robotics, mechatronics, autonomous systems, and mechanical design.

The project also demonstrated the importance of iterative testing and manufacturing-aware design. Future improvements could include a stronger tail structure, protected control linkages, better launch-string clearance, and more systematic evaluation of the control system. Collaboration with students and instructors at Nagoya University also strengthened technical communication, teamwork, and adaptability in an international engineering environment.

ACKNOWLEDGEMENTS

The author would like to express sincere appreciation to Professor Susumu Hara of the Control Systems Engineering Laboratory for his support throughout the SILP glider project. Gratitude is also extended to the laboratory teaching assistants and students for their assistance with design, manufacturing, programming, testing, and technical discussions. Appreciation is further given to the SILP organizers for providing the opportunity to study at Nagoya University and participate in the flight competition at Gifu University.

REFERENCES

[1] Airfoil Tools, “Airfoil Database and XFOIL Polar Diagrams.” [Online]. Available: https://airfoiltools.com/. Accessed: Jul. 16, 2026.

[2] Dassault Systèmes, “SOLIDWORKS for Students: 3D CAD Software for Education.” [Online]. Available: https://www.solidworks.com/product/students. Accessed: Jul. 16, 2026.

[3] Arduino, “Arduino IDE.” [Online]. Available: https://docs.arduino.cc/software/ide/. Accessed: Jul. 16, 2026.

[4] Nagoya University, Design and Drafting III: Flight Robot—2025 Design and Drafting III Guidance, English translation of the original Japanese slides, 2025.